Journal of Catalysis 256 (2008) 204–214

Contents lists available at ScienceDirect

Journal of Catalysis

www.elsevier.com/locate/jcat

Optimization and scale-up of CNF production based on intrinsic kinetic data obtained from TEOM

I. Kvande, D. Chen *, Z. Yu, M. Rønning, A. Holmen

Department of Chemical Engineering, Norwegian University of Science and Technology, NTNU, N-7491 Trondheim, Norway

ARTICLE INFO

Article history:
Received 17 November 2007
Revised 11 March 2008
Accepted 13 March 2008
Available online 29 April 2008

Keywords:
Carbon nanofibers
Ni
Methane decomposition
TEOM
Reaction mechanism
Scale-up

ABSTRACT

Optimizing the operating parameters for growing carbon nanofibers (CNFs) is an important step toward the large-scale production of CNFs with a high degree of structure control. The present work demonstrates that a tapered-element oscillating microbalance (TEOM) is an excellent tool for the kinetic study of the highly dynamic process of CNF growth. Initial CNF growth rates, deactivation rates, and yields can be studied simultaneously as a function of temperature, pressure, hydrogen partial pressure, or residence time. The kinetic data from TEOM studies are directly implemented to scale up the production of CNF. For a hydrotalcite (HT)-derived Ni catalyst (77 wt% Ni), the highest CNF growth rate was obtained at a temperature of around 580 °C and a hydrogen partial pressure of around 0.1 bar. High temperatures and low partial pressures of hydrogen resulted in a high initial growth rate and deactivation rate, whereas low temperatures and high partial pressures of hydrogen resulted in low initial growth rate and deactivation rate. A carbon capacity (maximum carbon yield) of 50 g/g cat could be achieved at optimized conditions. Growth rates and CNF yields were found to increase with increasing total pressure (0.3–3.8 bar). The mechanisms of CNF growth and deactivation were explored based on kinetic data and DFT calculation studies from the literature. The results obtained from the TEOM studies were verified in a PFR fixed-bed reactor and a horizontally placed fixed-bed reactor similar to a CSTR reactor. The residence time of methane was identified as the most important parameter for scaling up the process. The data on the effect of hydrogen from the TEOM were reproduced, and a successful scale-up of 10,000 times was achieved.

1. Introduction

Carbon nanofibers (CNFs) and carbon nanotubes (CNTs) have recently gained much interest in a series of applications due to their unique properties [1]. In the present study, CNFs are considered to be carbon with a graphite sheet oriented at an angle $>0°$ and $<90°$ with respect to the fiber axis and with a diameter in the range of 10–500 nm. CNTs have graphite sheets oriented parallel to the fiber axis (0°). Large-scale synthesis and application of CNFs relies on reducing the production costs while controlling purity. Catalytic chemical vapor deposition (CCVD) is generally considered the most promising process for large-scale synthesis of CNFs and CNTs with a high degree of structure and property (i.e., electrical, mechanical, surface) control [2]. Alternative routes for CNT synthesis, such as laser ablation and arc discharge, are more energy-demanding and hence costly and also produce large amounts of byproducts [2]. The properties of CNTs are in most aspects superior to CNFs, but the fundamentals governing their growth by CCVD from hydrocarbon decomposition (e.g., the effect of H_2 on the growth process) are similar.

Because of its abundance and low cost, methane is normally considered the best feedstock for CCVD. Methane decomposition also has been considered as an alternative route to produce CO-free H_2 with CNFs as an additional product [3–6]. Much effort has been devoted to gain insight into the CNF growth mechanism to optimize the synthesis process. The effects of metal catalyst and support characteristics [7–15], synthesis conditions [13,16–20], and different reactor systems [4,21,22] on the CNF growth have been investigated. Hydrotalcite (HT)-derived catalysts have been considered a viable choice for large-scale synthesis of CNF, because going through the HT structure makes it possible to synthesize a high-loading catalyst with a high dispersion and narrow particle size distribution [23].

Although numerous studies have investigated CNF and CNT synthesis by CCVD, most of this research has focused on catalyst development and synthesis conditions through empirical studies, with less effort put into kinetic studies. This may be due to the complexity of the CNF growth process, in which the sample volume increases significantly, making a horizontal reactor the usual reactor of choice. However, because of gas bypass, this type of

* Corresponding author. Fax: +47 735 94080.
E-mail address: chen@chemeng.ntnu.no (D. Chen).

0021-9517/$ – see front matter
doi:10.1016/j.jcat.2008.03.015

reactor is not very suitable for kinetic studies. Conventional microbalances are commonly used for kinetic studies of CNF growth. This type of reactor has problems with bypass and poorly defined flow through the catalyst bed, making it almost impossible to obtain reliable kinetic data [24].

The deactivation of the catalyst particles is a crucial factor affecting the yield of CNFs and CNTs. A detailed understanding of this process based on data from experiments in conventional kinetic reactors remains a research goal.

In a tapered-element oscillating microbalance (TEOM), all of the reactants are forced to flow through the sample bed. The change in mass is recorded by measuring the frequency changes in the sample bed. TEOM has proven to be a reliable tool for kinetic studies of processes with mass change, even for very fast processes, due to its rapid gate time of 0.86 s. Recently, TEOM has been applied in several studies of CNT and CNF growth processes that have provided insight into the relevant growth and deactivation mechanisms [10,24–27].

An important parameter for CNF growth is the hydrogen concentration. Hydrogen is the by-product of CNF and CNT production by decomposition of methane or other hydrocarbons. Therefore, control of the hydrogen profile along the reactor is crucial for the scale-up of the CCVD process. Higher hydrogen partial pressure increases the adsorption of hydrogen and suppresses the dissociation of methane, and also increases the rate of gasification. In addition, an increased hydrogen partial pressure helps prevent metal encapsulation and deactivation through polymerization of surface carbon. The dependence of carbon yield on the P_{H_2}/P_{CH_4} ratio has been explored through both mechanistic [28–31] and experimental studies [10,17,22,32–36].

The present work involves a detailed TEOM-assisted kinetic study of CNF growth by methane decomposition on a HT-derived Ni catalyst (77 wt% Ni). Optimization of the growth conditions and important parameters is targeted with respect to obtaining the maximum CNF yield (i.e., capacity). At the same time, controlling the CNF structure (i.e., the graphene sheet angle with respect to the fiber axis) and diameter, as well as limiting the amount of amorphous carbon byproduct, are important issues. An improved understanding of the mechanism of CNF growth, particularly the mechanism of catalyst deactivation, is sought. The intrinsic kinetic data obtained in the TEOM reactor were further verified in two types of fixed-bed reactors with different scales to identify important parameters for process scale-up.

2. Experimental

2.1. Catalyst preparation

The Ni^{2+}–Al^{3+} HT catalyst was prepared by a method modified from a previous study [37]. $Ni(NO_3)_2{\cdot}6H_2O$ and $Al(NO_3)_3{\cdot}9H_2O$ were used as metal precursors, whereas Na_2CO_3 and NaOH acted as precipitates. For the preparation, stoichiometric amounts of Na_2CO_3 and NaOH were dissolved in 400 ml of deionized water. A second solution containing $Ni(NO_3)_2{\cdot}6H_2O$ and $Al(NO_3)_3{\cdot}9H_2O$ dissolved in 375 ml of water was pumped slowly into the first solution under vigorous mechanical stirring. After the addition was complete, the gel was adjusted to pH 8.5 with nitric acid and aged at 80 °C for 15 h. The cooled sample was suction-filtered, washed repeatedly with large amounts of water, and vacuum-dried at 70 °C overnight. The Al^{3+}/Ni^{2+} was maintained at a ratio of 0.25. The as-prepared catalysts were calcined under a 100 ml/min flow of air at 480 °C for 15 h (5 °C/min). The catalyst used in the TEOM experiments was sieved to a size of 100–145 μm.

2.2. Catalyst characterization

X-ray diffraction (XRD) analysis was carried out using a Siemens D5000 X-ray diffractometer with Cu-K_α radiation through a primary monochromator. The resulting peaks were analyzed with a profile-fitting program (SIEMENS DIFFRAC^{plus} PROFILE), and crystal size and microstrain software (DIFFRAC^{plus} WIN-CRYSIZE) [38]. LaB_6 was used as a standard. Details on the method used to determine the particle size and particle size distribution are available elsewhere [39]. For characterization of the reduced sample, the metal oxides were reduced to the metallic state in a 1:1 N_2/H_2 mixture (total flow, 200 ml/min) for 15 h at 600 °C. After the reduction step, the samples were cooled to room temperature under flowing N_2 and passivated in an air/N_2 mixture (4 vol% air; total flow, 100 ml/min) for 2 h to prevent bulk oxidation of the catalysts.

Temperature-programmed reduction (TPR) of the calcined HT-derived catalyst was carried out in a in-house-built equipment [40]. The catalyst was loaded into a U-shaped quartz reactor. The temperature was measured with a thermocouple situated about 1 cm above the sample. The furnace temperature was controlled by a thermocouple located on the outside of the reactor. The samples were first reduced in 30 ml/min 7% H_2/Ar for 1.5 h at 600 °C. After the samples were cooled to room temperature, the TPR experiment was conducted by ramping the temperature at a rate of 10 °C/min until 900 °C in the same gas flow as for the reduction treatment. The consumption of hydrogen was determined by comparing the conductivity of a reference gas and the product gas in a Shimadzu GC-8A gas chromatograph. Calibration was performed using Ag_2O. N_2-adsorption measurements were carried out after evacuation to 50 Torr using a Micromeritics Tristar 3000 apparatus. Hydrogen chemisorption was conducted at 35 °C in a Micromeritics ASAP 2000 using 0.3 g of prereduced catalyst.

2.3. Synthesis of CNFs in TEOM

The effects of total pressure, H_2 partial pressure, residence time, and temperature were studied in a TEOM reactor (supplied by R&P, USA). A description of the TEOM and the experimental setup is available elsewhere [10]. Samples (2–10 mg) of a HT-derived Ni catalyst with 77 wt% Ni were inserted in the reactor. A large void volume was maintained to avoid pressure drop in the reactor. The catalyst was reduced in a 50 mol% H_2/Ar mixture at 580 °C for 8 h (2 °C/min), then flushed in Ar for 10 min. Synthesis was carried out at atmospheric pressure.

A gate time of 0.84 s was set to record the mass of the sample. Accordingly, the mass changes were calculated every 0.84 s. One of the main advantages of the TEOM in studying kinetics of CNF growth is that it can directly and frequently measure both accumulated mass and relatively small mass changes simultaneously. For the hydrogen partial pressure experiments, the flow rate of methane was kept constant at 100 ml/min and diluted with Ar. Experiments were carried out at 580 and 600 °C at 0.3 bar methane partial pressure. The hydrogen partial pressure was adjusted by replacing Ar with hydrogen at constant total pressure. The effect of temperature was studied in the range of 500–620 °C. Pressure effects were investigated at 0.34, 0.9, and 3.78 bar. The effect of residence time was indicated by experiments at a methane flow of 12 and 45 ml/min $CH_4(90)/N_2(10)$. The accumulation of CNFs and the growth rates were recorded every minute. For the rapid formation of CNFs, these data can be recorded at time intervals as short as 0.84 s.

2.4. Scale-up of CNF synthesis

The results of the TEOM studies were used to set up a series of experiments in two fixed-bed reactors. The HT-derived Ni catalyst

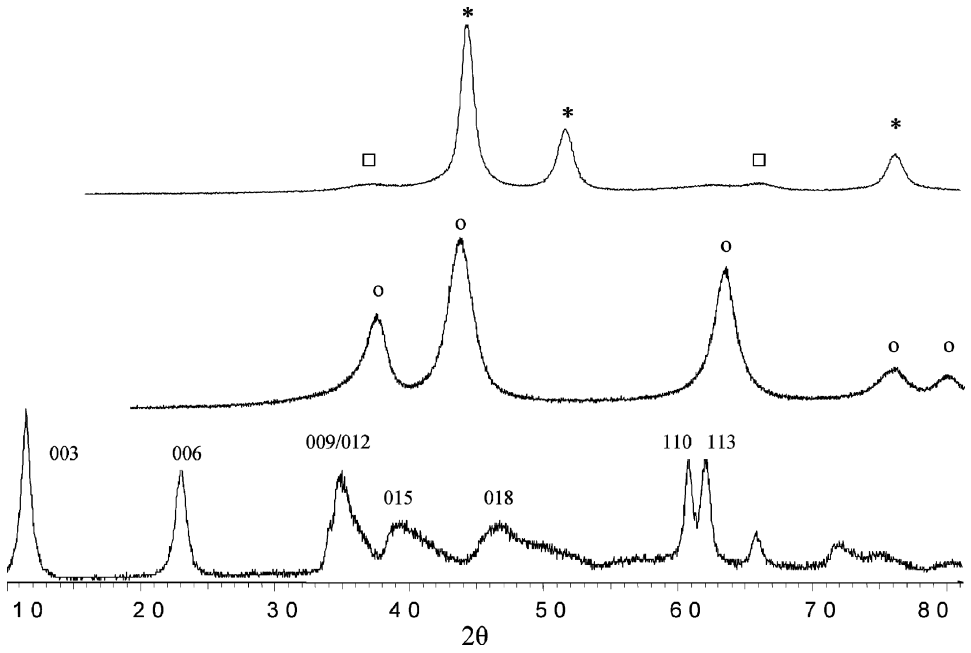

Fig. 1. XRD patterns for the HT and HT-derived materials. From bottom to top: as-prepared hydrotalcite (different planes marked), calcined sample, NiO (o), and reduced and passivated sample, fcc Ni (*) and γ-Al_2O_3 or spinel $NiAl_2O_4$ (□).

was reduced in 25% H_2/N_2 at 600 °C for 1.5 h, simplifying pretreatment of the catalysts. Synthesis was performed at 600 °C in both a fixed-bed setup using a quartz reactor (4 cm i.d.; 25 cm long) and a large-scale ceramic reactor (8 cm i.d.; 60 cm long). The quartz reactor was vertically oriented with a bottom inlet; all the gas passed through the catalyst bed. The ceramic reactor was horizontal; the catalyst was placed in a quartz boat. Weight hourly space velocities (WHSVs) of methane ranging from 4.6 to 1600 l/g_{cat} h, corresponding to different conversion levels and thus different partial pressures of hydrogen, were used. A higher WHSV resulted in a lower conversion and lower hydrogen partial pressure. The reactant mixture was analyzed by an Agilent 3000 online micro-gas chromatograph.

2.5. Flow pattern experiments

Pulse injection experiments were performed to determine the typical flow patterns for the two scale-up reactors. Nitrogen was fed continuously, and a pulse of H_2 was injected. The outlet concentration was determined by an online gas chromatograph, with an analysis interval of 1 min.

2.6. Characterization of CNFs

A JEOL 2010F electron microscope equipped with a field emission gun was used to characterize some of the synthesized CNFs by TEM. The samples were prepared by ultrasonic dispersion of the CNF in ethanol. A drop of the solution was applied onto a holey carbon support grid.

3. Results and discussion

3.1. Catalyst characterization

The preparation of a highly loaded, well-dispersed Ni catalyst is challenging but essential for synthesizing high yields of CNFs. By going through an HT structure prepared by coprecipitation, a thermally stable catalyst with a high surface area and high Ni dispersion can be obtained [23]. The catalyst will have small particles with a narrow size distribution, of great importance because the CNF diameter is proportional to the initial Ni particle diameter [10]. Higher yields can be obtained with other catalyst systems, such as unsupported metal particles [7,41] but the product tends to have wider CNF diameter distributions and to be less well defined. XRD patterns for the as-prepared, calcined, and reduced catalyst are shown in Fig. 1. The diffraction pattern for the as-prepared catalyst shows the HT structure as the only crystalline component, exhibiting sharp and symmetric reflections for the basal (003) and (006) at 2θ of 11° and 22.5°. The reflections of the basal (009) and nonbasal (012) planes are seen at around 35°. Asymmetric reflections of the (015) and (018) nonbasal planes are seen at 2θ of 39° and 41.5°. There are no peaks corresponding to either hydroxide or carbonate compounds. The diffraction pattern of the sample calcined at 480 °C corresponds to crystalline NiO. Incorporation of Al into the lattice of NiO is very likely, because the incorporation of other metals into NiO has been reported for other HT structures [42]. The presence of Al in the vicinity of the highly dispersed metal atoms prevents sintering. After reduction of the calcined material, the XRD pattern corresponds to fcc Ni; however, some minor peaks are seen at a 2θ of 37° and 66° that correspond to either γ-Al_2O_3 or $NiAl_2O_4$ spinel. Fig. 2 shows the crystal size distribution analysis for the reduced catalyst as determined from the PROFILE program [38], assuming a Pearson VII function for the peak profile fitting. The almost-pure HT-derived Ni/Al_2O_3 has a Gaussian-like particle size distribution; the average particle size is 5.0 nm, whereas the particle size determined by chemisorption is 16 nm. The discrepant findings of these two methods may be due to incomplete reduction of the catalyst in the chemisorption experiment. A size discrepancy between XRD and chemisorption measurement also has been seen in studies of similar HT structures [23]. Additional Ni particle size characterization by TEM gave a size similar to that determined by chemisorption [23]; therefore, it seems likely that the size obtained from XRD is an underestimate. A detailed chemisorption study (results not shown here) demonstrated that a prolonged reduction time had no significant effect on Ni particle size; this can be explained by the catalyst's high thermal stability. Thus, the extra time needed for the reduction step in the XRD and chemisorption experiments compared with the TEOM and scale-up experiments would not be expected to change the particle diameter and shape significantly.

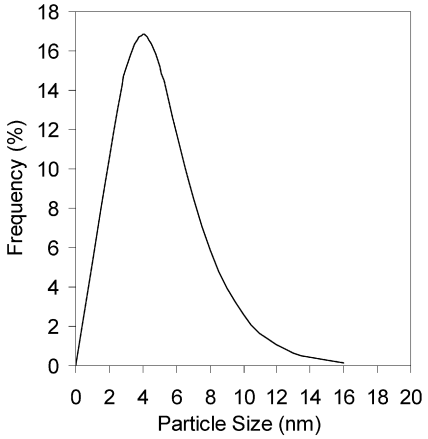

Fig. 2. Nickel particle size distribution of the reduced HT-derived catalyst as determined by XRD and the software WIN-Crysize [38,39].

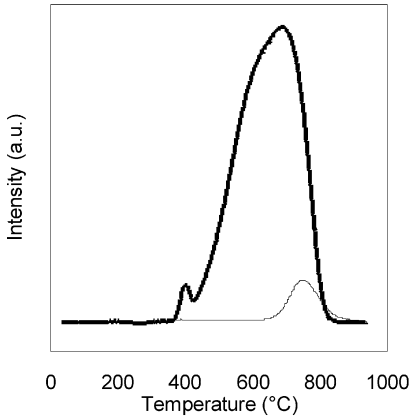

Fig. 3. Temperature-programmed reduction (TPR) profile of the calcined catalyst (bold) and the catalyst reduced at the same conditions as the scale-up experiments; 25% H_2/N_2 at 600 °C for 1.5 h (simple).

The surface area of the same type of HT structure was found to increase from 139 to 165 m^2/g with calcination, with an increase in pore volume from 0.20 to 0.34 cm^3/g [43]. This is attributed to the formation of pores and channels caused by the removal of H_2O and CO_2 [44]. Reduction of the calcined material led to a decrease in the surface area to 90 m^2/g, due mainly to the collapse of pores [43].

Fig. 3 shows the TPR profile for the calcined catalyst. The weak peak seen at 435 °C may be ascribed to the presence of small amounts of Ni^{3+} species in the external layers of the solids [42]. The main H_2 uptake exhibits a continuous broad peak from 460 to about 860 °C, possibly related to the highly dispersed NiO particles that are reduced over a wide temperature range [45]. Pure NiO was reduced at a much lower temperature than HT-derived NiO. The higher reduction temperature for HT-derived NiO can be attributed to the presence of Al^{3+} ions inside the oxide phase [46]. The catalysts used in the CNF synthesis were reduced at 580 °C for 8 h in the TEOM reactor and at 600 °C for 1.5 h in the scale-up experiments. Reduction of the calcined material readily occurred at ca. 600 °C, as shown by the TPR profile. Fig. 3 also shows the TPR profile of a catalyst prereduced at the same conditions as for the scale-up experiments. The unreduced fraction at the current reduction conditions could be difficult-to-reduce $NiAl_2O_4$, as demonstrated by XRD. The scale-up reduction conditions are considered sufficient for this study, because only a relatively small amount of Ni was left unreduced at high temperatures, as shown by the TPR experiments.

3.2. Synthesis of CNFs in TEOM

3.2.1. Effect of temperature

The effect of temperature on the carbon yield was studied. The results, shown in Fig. 4, demonstrate that both the growth rate and the CNF capacity (i.e., maximum carbon yield) increased as the temperature was raised from 500 to 580 °C. This can be explained by the increased rate of the surface reactions, which led to a higher CNF growth rate. The rate was highest at 580 °C, resulting in a CNF yield of 50 g/g of catalyst, with the capacity decreasing substantially at higher temperatures. A temperature increase of only 40 °C resulted in a carbon yield approximately 5 times lower than that at the optimum temperature. A similar temperature dependence was found by Avdeeva et al. [8] and Reshetenko et al. [47]. A 90 wt% Ni/Al_2O_3 catalyst achieved a yield of 145 g/g cat at 550 °C, whereas a low CNF yield (<20 g/g cat) was found at 625 °C. The lower CNF yield obtained at higher temperatures was due to more rapid deactivation, as also seen in Fig. 5. The CNF growth rate is plotted in Fig. 5a, and the deactivation function (r/r_0, where r and r_0 are the CNF growth rates at TOS of t and 0, respectively) as a function of TOS is plotted in Fig. 5b.

Although the deactivation mechanism of CNF growth has been studied extensively, the findings reported in the literature are inconsistent. In some studies, induction, acceleration, and deactivation periods have been observed [8,9,30], whereas other studies found no induction and deactivation periods [28,48]. It has been suggested that the gas-phase affinity for carbon formation is an important parameter in controlling carbon nucleation and growth, and that a low partial pressure of methane (or high partial pressures of H_2) results in an induction period [28,30,48]. Fig. 5b shows

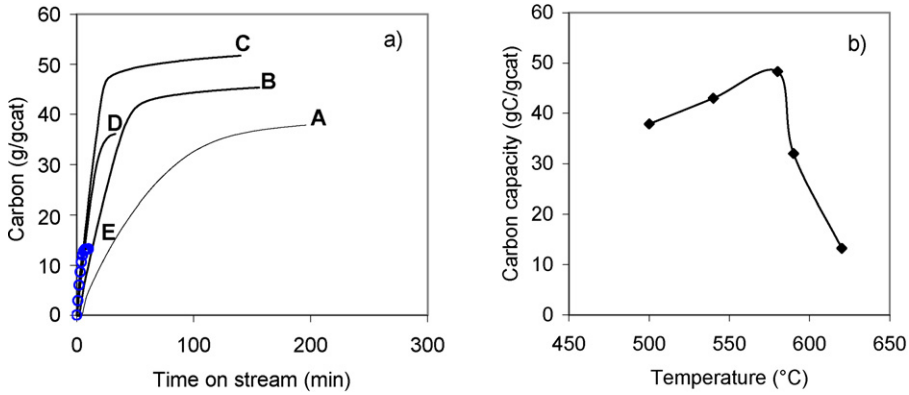

Fig. 4. (a) Carbon (g C/g cat) as a function of time on stream during CH_4 decomposition in TEOM at 500 °C (A), 540 °C (B), 580 °C (C), 590 °C (D), 620 °C (E). (b) Carbon capacity as a function of temperature during CH_4 decomposition in TEOM. Flow conditions: 45 ml/min $CH_4(90)/N_2(10)$, 5 ml/min H_2.

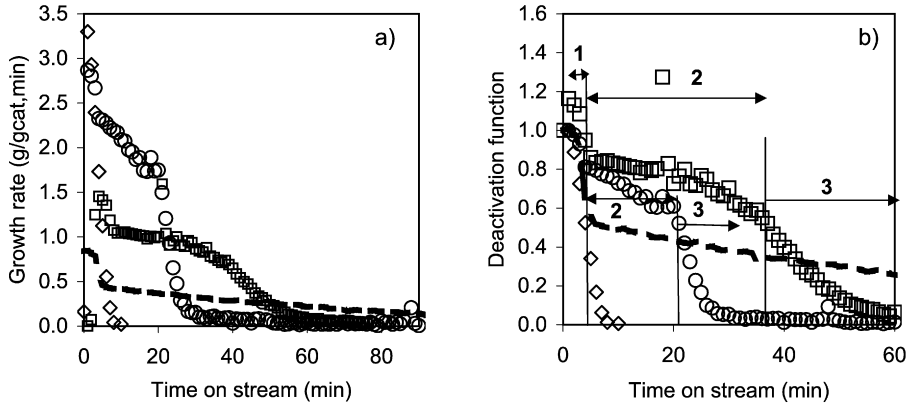

Fig. 5. (a) Growth rate and (b) deactivation function (r/r_0; r and r_0 are the CNF growth rates at time on stream of t and 0, respectively) at different temperatures: 500 °C (– –), 540 °C (□), 580 °C (○), and 620 °C (◇) as a function of time during CH_4 decomposition in TEOM. The labeled regions in (b) refers to 1: rapid deactivation, $t < 6$ min, 2: steady state growth, 3: encapsulation of the catalyst particle.

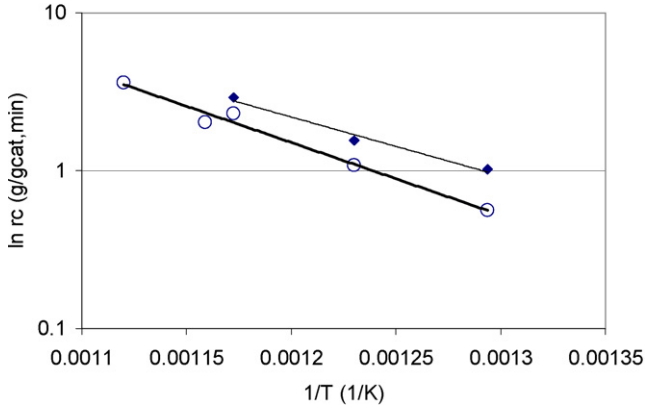

Fig. 6. Arrhenius plots for region 1 (■) and region 2 (○) shown in Fig. 5. The data sets for a series of experiments at lower temperatures were extrapolated to $t = 0$ to find the "initial" reaction rate at each temperature.

a complicated deactivation behavior of the HT-derived Ni catalysts, including three main characteristic regions of CNF growth. At the start of the experiment, a rapid transition occurred from one reaction period (region 1) to a steady-state growth-like behavior (region 2). The initial growth rate (region 1) was higher than the steady-state rate (region 2). Steady-state growth was followed by a decrease in growth rate caused by deactivation of the catalyst (region 3). Note that the accurate measurements of growth rate in TEOM, combined with the differential operation methane conversion of <5%, makes it possible to study the kinetics of CNF growth, including deactivation in detail. For the first time, the initial period of growth can be investigated.

We attempted to analyze the data with respect to the distinct changes in the growth process behavior shown in Fig. 5. The data sets for the series of experiments at lower temperatures was extrapolated to $t = 0$ to find the "initial" reaction rate for the two first characteristic reaction periods at each temperature. At temperatures above 590 °C, the first region was not obtained, because the first data point was recorded after 1 min. Therefore, here the initial growth rates corresponding to region 1 are presented only for temperatures below 590 °C. An activation energy plot of these data is shown in Fig. 6. The initial reaction period had a lower activation energy (64.6 kJ/mol) compared with the steady-state period (92.4 kJ/mol). Both activation energies were in the same range as for other studies, in which values from 50 to >100 kJ/mol have been reported. The value obtained at steady state corresponds well to the values of 90 kJ/mol found at 450–590 °C [29] and 97 kJ/mol at 530–590 °C [31], in contrast with previously reported activation energies of 46 kJ/mol [30], 60 kJ/mol [28], and 75 kJ/mol [16]. The wide range of reported activation energies may be due to many factors, including the difficulty of collecting true kinetic data and the highly dynamic characteristics of the process. Because the deactivation is fast and the effect of hydrogen is significant, the data collection must be done rapidly. Trustworthy data can be obtained only with no bypass at low conversion and with the possibility of fast analysis. In this respect, the TEOM reactor has been recognized as an excellent tool for kinetic studies of reactions in which rapid deactivation occurs by carbon or coke formation [24,49]. Another important factor is the highly dynamic nature of the growth process, in which the activation energy can change with TOS, as discussed earlier.

There is an ongoing debate concerning the mechanism of carbon diffusion for CNF growth. It is generally accepted that carbon diffusion through the bulk of the metal particle is a critical step in CNF growth, based on the fact that the measured activation energy of CNF growth is similar to the activation energy of carbon diffusion through the metal particles [9,50]. But this supposition has recently been challenged by in situ TEM observations as well as DFT calculations. DFT calculation studies by Abild-Pedersen et al. [51] identified Ni step edges as important metal–carbon adsorption sites for CNF growth from methane decomposition; thus, surface diffusion was found to be more energetically favorable compared to bulk diffusion. The calculated activation energy of surface diffusion was 0.5 eV (1 eV ∼ 100 kJ/mol) on Ni (111) and 0.55 eV for diffusion from step edges to the clean surface. A significantly higher activation energy of 1.8 eV was found for bulk diffusion, which was considered unlikely for this process [51].

Based on the TEOM results shown in Fig. 5b, the initial growth rate was high, but deactivation was rapid, implying that the mechanism of growth changed abruptly during the initial period of CNF growth. The activation energy in this initial growth period (64.6 kJ/mol, as determined by TEOM experiments) was close to the DFT-predicted value on surface diffusion. This may correspond to the surface diffusion on Ni (111) being a dominating (i.e., more likely) diffusion path on relatively fresh and unspoiled Ni surfaces. DFT calculations showed step sites to be highly active; that is, the carbon binding energy on Ni (211) steps was considerably greater than on Ni (111) [51,52]. The high carbon binding energy corresponds to a low activation energy of methane decomposition, which in turn gives higher surface reaction rates. At the same time, these sites are more prone to deactivation, because a high binding energy will result in blockage of step sites by strongly bonded carbon atoms. This effect will be very pronounced at the high rates of methane decomposition seen at high temperatures and high methane partial pressures. Fig. 5b shows that the second region,

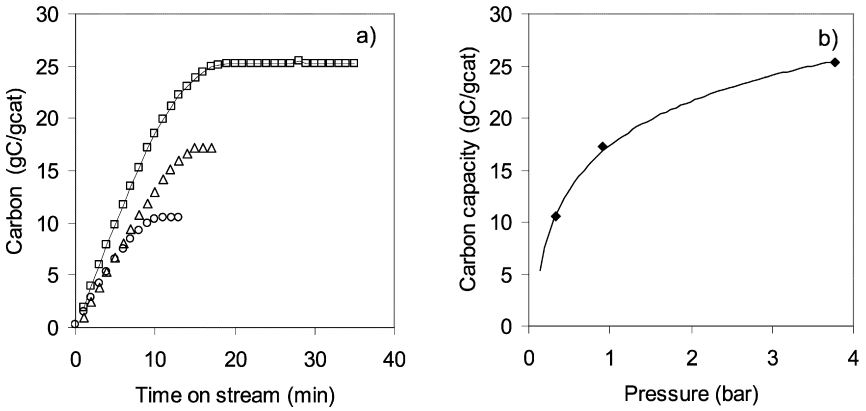

Fig. 7. (a) Carbon (g C/g cat) as a function of time on stream. (b) Carbon capacity as a function of pressure at: 0.34 (○), 0.90 (△) and 3.78 bar (□). Experimental conditions: 580 °C, CH_4:N_2 = 90/10, obtained during CH_4 decomposition without H_2 in TEOM.

although displaying a lower CNF growth rate, was relatively stable. The activation energy of 92.4 kJ/mol of the steady-state growth region does not correspond to the values for surface diffusion calculated from DFT studies [51].

Previous kinetic studies [9,53,54], as well as high-resolution TEM investigations [55,56], have clearly demonstrated a significant reconstruction of Ni particles during methane decomposition. Yang and Chen [54], through experimental and theoretical studies on CNF growth, verified that the Ni (100) and Ni (110) surfaces are gas–metal interface sites, whereas the Ni (111) and Ni (311) surfaces are graphite–metal interface sites [54]. Zhu et al. [57] recently investigated the adsorption and diffusion on the surface and subsurfaces of Ni (100) by DFT calculations and found a high activation energy of 1.97 eV for C surface diffusion on Ni (100), with an activation energy of 1.57 eV for subsurface C diffusion. Increasing the surface carbon concentration from 0.1 to 0.43 ML induced a "clock" reconstruction of the Ni (100) atoms, increasing the volume of the subsurface site and allowing more C to dissolve in the Ni bulk. An activation energy of 1.16 eV was found, not very different from the activation energy of 92.4 kJ/mol obtained for steady-state growth of CNFs. Other DFT calculations on C diffusion in bulk Ni particles indicated that the activation energy was highly dependent on the concentration of C in the Ni bulk particles [58], decreasing from 1.64 eV in $Ni_{32}C$ to 1.26 eV in Ni_4C and further to 0.972 eV in a $Ni_{32}C_8$ supercell, which is very similar to the experimentally determined activation energy for the steady state growth period obtained in the present work. The DFT calculations and TEOM results suggest that the experimental activation energy and the mode of diffusion are highly dependent on the growth conditions, specifically the carbon surface coverage.

Multiple mechanisms, including blocking of catalyst sites and fragmentation of catalyst particles, have been suggested as possible explanations for the deactivation of the CNF growth catalyst. In addition, deactivation has been linked to substantial elongation and capture of Ni particles inside the carbon filaments [30]. In the present study, the formation of encapsulating carbon is considered the main cause of deactivation. This aspect has been previously discussed assuming that surface atomic carbon is a common intermediate for both the main reaction and encapsulating carbon formation during dry reformation of methane [25]. The formation of encapsulating carbon was considered an irreversible reaction between adsorbed carbon atoms. Thus, the encapsulating carbon formation process can be written as

$$n^{**}C \rightarrow nC_p, \tag{1}$$

$$r = k_p q_c^n, \tag{2}$$

where k_p is the rate constant for encapsulation and q_c is the carbon surface coverage. The rate constant increases with temperature, and the site coverage increases with an increasing rate of methane decomposition. An ensemble size of 6 for the encapsulating carbon formation was obtained based on Eq. (2) and previous experimental data [25]. Figs. 5a and 5b similarly indicate that a threshold exists for the formation of encapsulating carbon as the steady-state period is followed by rapid deactivation. The results depend on the ensemble size. As long as the formation of larger ensembles of encapsulating C is depressed, the deactivation rate can be limited, because sufficient carbon site coverage is required for nucleation of the hexagonal carbon ring. Higher temperatures result in greater carbon surface site coverage, thereby leading to higher deactivation rates, as shown in Fig. 5b. Once the graphitic shells are formed on the Ni particles, the Ni catalyst is completely deactivated. The TEOM results demonstrate that the deactivation process depends on the kinetic balance among all of the steps involved. Fig. 5b illustrates this by the different deactivation behavior at 500 °C compared with that at higher temperatures. No stabilized growth region is observed, and the catalyst deactivates continuously, possibly due to the lower diffusion rate and/or lower carbon solubility. These findings indicate that obtaining high CNF yields requires a delicate balance among surface reaction, dissolution, and diffusion.

3.2.2. Effect of total pressure

The effect of pressure on the carbon yield is illustrated in Fig. 7. An increase in methane partial pressure had a significant influence both on the CNF growth rate and the rate of deactivation; whereas the growth rates were similar at 0.34 and 0.9 bar, a considerably higher rate was seen at 3.78 bar. Demicheli et al. [59] reported a linear increase in growth rate for methane decomposition at increasing pressure. Snoeck et al. [48] also found a higher rate of carbon formation at increasing pressure when studying methane decomposition on Ni at 1.5, 5, and 10 bar. These authors emphasized that varying the partial pressure induced changes in equilibrium carbon surface coverage due to competition between gas adsorption and solid segregation. An increased pressure increased the surface coverage of methane and thereby the rate of surface reactions and the growth rate; however, the increase in the rate seemed to level off at higher pressures. The authors suggested that any further increase in the rate was impeded by saturation of methane on the surface.

Fig. 8 shows a significantly reduced rate of deactivation with a pressure increase from 0.34 to 0.9 bar, but with a similar deactivation rate at pressures of 0.9 and 3.78 bar. These results demonstrate the complicated effect of pressure. The differences can be

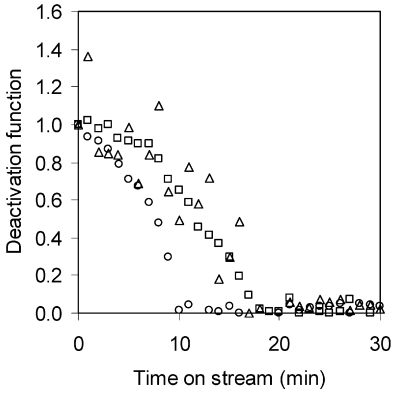

Fig. 8. Deactivation function (r/r_0; r and r_0 are the CNF growth rates at time on stream of t and 0, respectively) as a function of time on stream for CH_4 decomposition in TEOM at: 0.34 (○), 0.90, (△), and 3.78 bar (□). Experimental conditions: 580 °C, CH_4:N_2 = 90/10, no H_2.

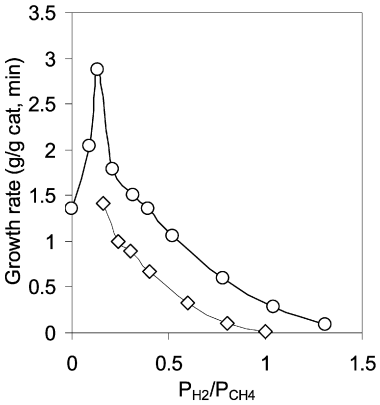

Fig. 10. Growth rate as a function of the H_2/CH_4 ratio at 580 (○) and 600 °C (◇) found in TEOM experiments.

tentatively explained by the competitive adsorption of H, C, and CH_x species.

3.2.3. Effect of H_2 partial pressure

The effect of hydrogen concentration has been studied extensively for systems using various carbon sources [17,22,32–36,48]. Hydrogen has been reported to both accelerate [32–34,36] and suppress [22] CNF formation. A decreased rate of carbon formation with increasing hydrogen partial pressures was found by Snoeck et al. [48], attributed to an increased gasification rate or a decreased affinity for carbon formation due to a more difficult basis for nucleation. Along with suppressing the dissociation of methane and increasing the rate of gasification, hydrogen adsorption increased with increasing hydrogen partial pressure. In addition, the increased surface coverage of H_2 helped avoid the polymerization of adsorbed C species that can encapsulate and deactivate the catalyst. Fig. 9a shows that the carbon capacity was 2.5 times higher with 5 ml/min H_2 in the feed than with no H_2 in the feed. The deactivation function plotted in Fig. 9b illustrates the less-pronounced deactivation at high hydrogen partial pressure. As shown in Fig. 10, the results from the TEOM experiments at different hydrogen partial pressures indicate a significant effect of hydrogen partial pressure on the growth rate. An optimum hydrogen partial pressure exists with respect to growth rate, over which the rate decreases significantly. At low methane partial pressures, the suppression of encapsulating carbon formation dominates and the growth rate increases; however, at some point, an increased rate of gasification, a lower rate of methane dissociation, and competitive H_2 adsorption dominate, and the growth rate decreases. An optimum hydrogen concentration also has been determined for a similar system, with the highest growth rate occurring at 50% H_2 [17].

3.2.4. Effect of residence time

Because hydrogen is a product of methane decomposition, the residence time of methane in the reactor has a significant effect on the growth. Fig. 11 plots the carbon capacity as a function of time for methane feeds of 12 and 45 ml/min $CH_4(90)/N_2(10)$. A higher reactant total flow (shorter residence time) increased the carbon capacity. More specifically, the shorter residence time resulted in lower methane conversion and thereby a lower hydrogen concentration and a higher growth rate, corresponding to the trend shown in Fig. 10. Fig. 11b shows the deactivation function plot. Note that although a higher growth rate was obtained at shorter residence times, catalyst deactivation was faster. At shorter residence times, the H_2 level dropped, thereby increasing the rate of encapsulating carbon formation. Tuning of the H_2 concentration level by controlling the residence time is crucial to obtain the optimal growth rate and carbon capacity.

3.3. Scale-up of CNF synthesis

The TEOM experiments revealed a temperature of 580 °C and a pressure somewhat higher than 1 bar as the preferred conditions for CNF growth. In addition, the analysis of the TEOM results indicated that hydrogen partial pressure or conversion level was the most influential parameter for the scale-up of the CNF growth process, because hydrogen is a byproduct of CNF growth. The hydrogen generated during the process would be expected

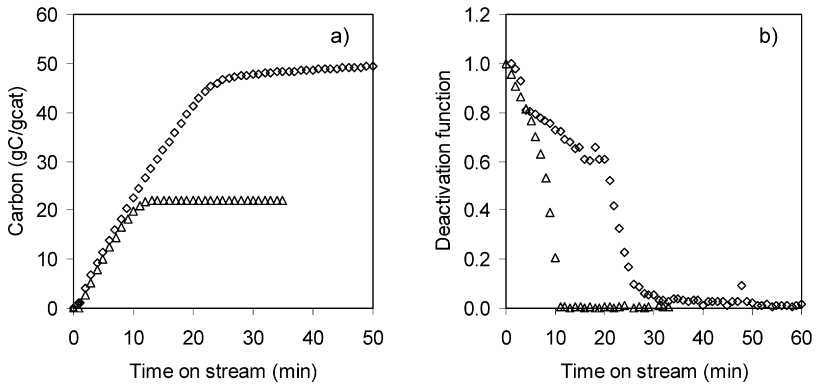

Fig. 9. (a) Carbon (g C/g cat) as a function of TOS and (b) deactivation function (r/r_0; r and r_0 are the CNF growth rates at time on stream of t and 0, respectively) as a function TOS with 0 (△) and 5 ml/min H_2 (◇) obtained from TEOM.

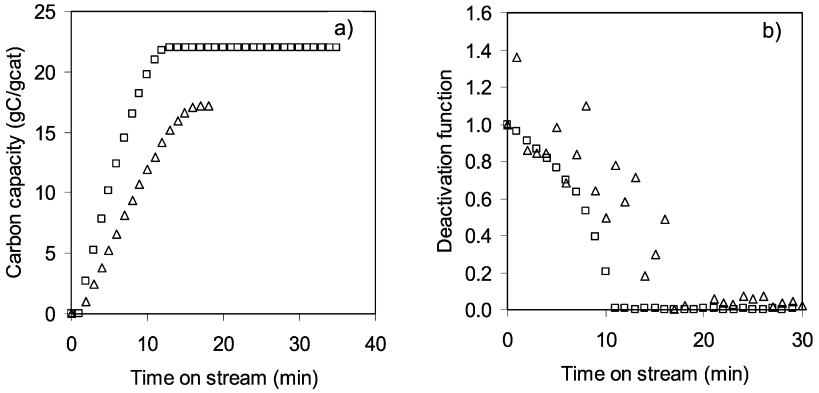

Fig. 11. (a) Carbon capacity and (b) deactivation function (r/r_0; r and r_0 are the CNF growth rates at time on stream of t and 0, respectively) as a function of time on stream for H_2 flows of 12 ml/min (△) and 45 ml/min (□) $CH_4(90)/N_2(10)$.

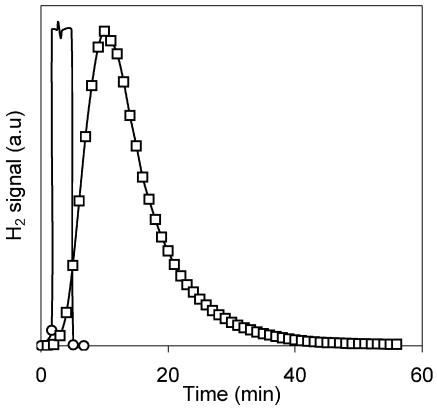

Fig. 12. Flow pattern as determined by injection experiments for the vertical quartz reactor (○) and horizontal ceramic reactor (□). Nitrogen was fed continuously, and a pulse of H_2 was injected. The outlet concentration was determined by an online GC with analyses every minute.

to significantly influence the growth rate. Most of the TEOM experiments were performed under differential conditions (i.e., at low conversion [<5%]). Two differently configured reactors—PFR and CSTR reactors—were designed as micro-pilot reactors for CNF synthesis to verify the TEOM results and identify the important parameters for scaling-up the process. Mini pilot plant experiments with different residence times at 1 bar were designed with the aim of verifying the experimental data on the effect of hydrogen on CNF growth found in the TEOM reactor. The effect of hydrogen on deactivation was addressed in experiments conducted in a CSTR reactor.

3.3.1. Flow pattern experiments

The scale-up experiments were done in a vertical quartz reactor and a horizontal ceramic reactor. Flow pattern experiments were performed to extract the correct data from the scale-up experiments. A pulse of H_2 was introduced in a continuous N_2 flow; the H_2 signal as a function of time is shown in Fig. 12. A long residence time for H_2 was found for the ceramic reactor, corresponding to the findings in the CSTR reactor. The pulse-like behavior of the vertical quartz reactor resembled a typical residence time plot for a plug–flow reactor. These findings were used to find the outlet pressure of H_2. The outlet concentration for the vertical quartz reactor can be approximated by $P_{H_2} = (P_{H_2,in} + P_{H_2,out})/2$, whereas for the ceramic reactor, $P_{H_2} = P_{H_2,out}$.

3.3.2. Scale-up results

Fig. 13a plots the growth rate as a function of the H_2/CH_4 ratio obtained from the scale-up experiments along with the growth rates obtained from the TEOM studies. These growth rates are in good agreement, with an increase in growth rate seen at shorter residence times. This can be explained in terms of the TEOM results discussed previously. A shorter residence time resulted in a lower H_2 partial pressure in the catalyst bed through a lower methane decomposition conversion, leading to a higher growth rate. However, Fig. 13b shows a decreasing carbon capacity at shorter residence times. There is an optimum residence time with respect to carbon capacity, corresponding to a WHSV of 410 l/g_{cat} h. These findings clearly indicate that an increase in the hydrogen-to-methane ratio decreased both the initial growth rate and the deactivation rate, in good agreement with the results from the TEOM experiments. A trade-off between initial growth rate and

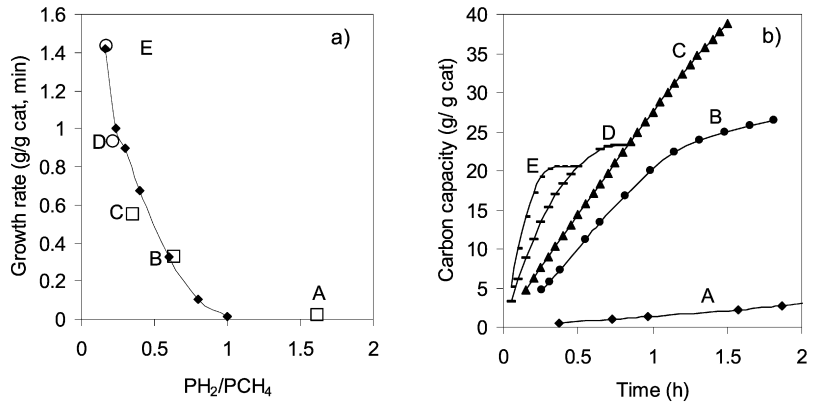

Fig. 13. (a) Growth rate as a function of H_2/CH_4 ratio and (b) carbon capacity as a function of time in TEOM at 600 °C (– –), at 600 °C in ceramic horizontal reactor (□; A [WHSV: 4.6 l/g_{cat} h], B [WHSV: 187 l/g_{cat} h], C [WHSV: 410 l/g_{cat} h]), and at 600 °C in vertical quartz reactor (○; D [WHSV: 738 l/g_{cat} h], E [WHSV: 1612 l/g_{cat} h]).

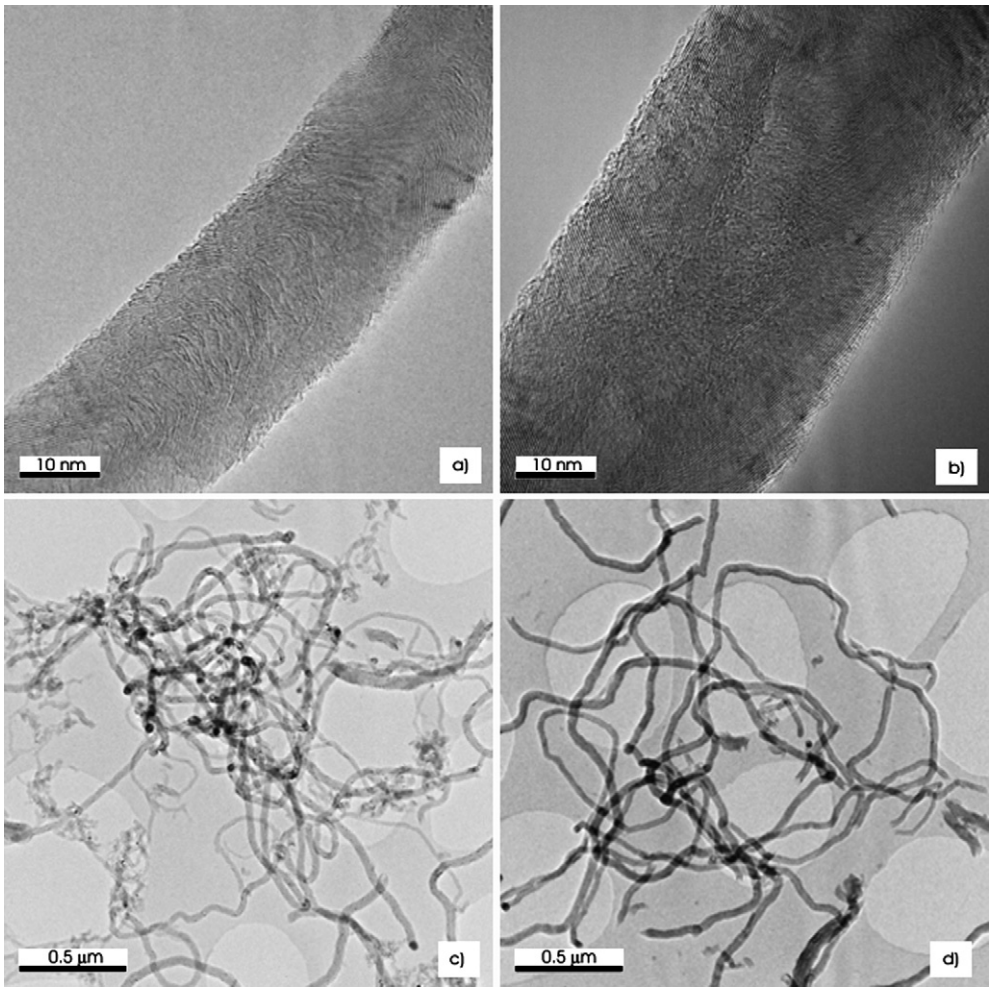

Fig. 14. (a) TEM image of typical CNF synthesized in TEOM. (b) TEM image of typical CNF synthesized in ceramic reactor. (c) Bundle of CNF synthesized in TEOM. (d) Bundle of CNF synthesized in ceramic reactor.

deactivation rate resulted in an optimum H_2-to-methane ratio of ca. 0.4 in terms of the best CNF yield.

The foregoing results demonstrate that the kinetic data obtained at an mg scale in the TEOM reactor were verified at very different scales using different reactors. This indicates that TEOM is a powerful tool for the kinetic study of CNF growth due to the high accuracy of the obtained intrinsic kinetic data, especially with respect to the direct measurement of growth rate at different conditions. The data collected from both the TEOM and the scale-up experiments provide a good basis for choosing a suitable reactor for CNF growth.

Keep in mind that a fixed-bed reactor is not the obvious choice as the reactor for evaluating CNF growth, even though such a reactor was used to verify the kinetic data from TEOM. The principles of the kinetic analysis are valid for all reactor types. The detailed design of the reactor depends on the purpose of the process, however. If CNF is the main product, then a hydrogen-to-methane ratio of ca. 0.4 is preferred. A moving- or rotating-bed reactor with a solids residence time of ca. 1–1.5 h with continuous addition of catalyst and removal of CNFs would be a good choice as a reactor for studying CNF growth. A fluidized-bed reactor also may be suitable, especially for obtaining the preferred hydrogen concentration throughout the entire reactor. Because the CH_4 conversion is relatively low at these conditions, a system for recycling the feed should be included. A hydrogen separation unit has been suggested to increase the methane conversion level [3]. H_2 can be removed by, for example, selective oxidation or through a membrane process. Because methane decomposition is highly endothermic, with CNF and hydrogen as the main products, a high temperature can be chosen to make hydrogen production more thermodynamically favorable. A high concentration of hydrogen in the reactor is then preferred to reduce the deactivation rate. Detailed kinetic and reactor modeling are necessary to design and optimize the reactor.

3.4. Characterization of the synthesized CNF

The diameter and structure of the CNFs were determined in a TEM study. Fig. 14a shows a TEM image of CNFs grown at 590 °C in the TEOM, and Fig. 14b shows a TEM image of CNFs grown in the ceramic reactor at 600 °C. The diameter distribution shown in Fig. 15 was determined by counting approximately 100 CNFs from low-resolution images, as shown in Figs. 14c and 14d for CNFs grown in the TEOM and the ceramic reactor, respectively. The mean CNF diameter was 24.5 nm in the TEOM sample and 35 nm in the scale-up experiment. These findings indicate that the CNFs synthesized in the TEOM were of a slightly smaller diameter. The difference may be due to the different H_2 profiles of the reactors, with the TEOM having a PFR profile and the large-scale reactor having a CSTR profile. Although the results seem to imply a possible effect of the reactor on the final CNF diameter, no strong conclusions can be reached, due to a standard deviation of almost 10 nm. The angles with respect to the fiber axis were similar in the CNFs from both experiments, ranging from 20° to 30°. The fiber diameter was considerably larger than the initial nickel

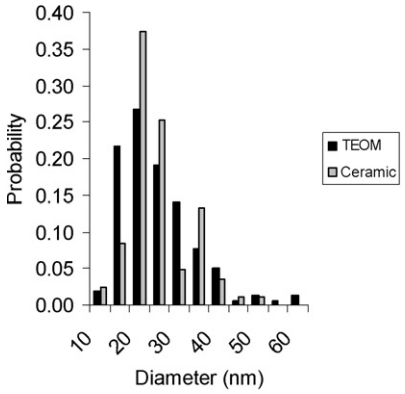

Fig. 15. Diameter distribution of CNF synthesized in TEOM and ceramic reactor.

particle size. This can be attributed to particle reconstruction in the initial stages of CNF synthesis [60].

Our findings demonstrate a slightly larger diameter for the CNFs produced in the scaled-up process, with the structure seemingly independent of the production scale. The scale of the reported CNF production reactor is typically ca. 200–300 g per batch in the fixed bed, compared with ca. 10 mg in the TEOM reactor. Thus, the present work has demonstrated a successful scale-up by a factor of about 10,000. In principle, a CNF yield of 50 g/g cat can be obtained during a reaction time of 20 min at optimal conditions.

In this respect, CNF structure control is a crucial factor—clear differences in, for example, electrical [61] and catalytic properties [39,62,63] have been reported among near-tube (0°), Fishbone (0–90°), and platelet (90°) CNFs. A narrow diameter distribution would be a natural goal for their utilization. For CNTs, the properties of deposited entities have been shown to be dependent on CNT curvature [64].

The present work has focused on how to optimize the process with respect to yield. The fishbone CNFs produced typically have a high crystallinity and low amorphous carbon content [65]. The edge structure available for interaction with and deposition of chemical species is low compared with that seen in CNFs with a higher average angle between the graphite sheets and the fiber axis. Numerous defects are required for successful interaction with chemical species for catalytic and composite applications; however, the high number of defects increases the instability of the CNF systems at higher temperatures and under oxidative conditions. Other structures (e.g., platelets, CNTs) can be obtained by changing the operation conditions (i.e., catalyst, feedstock, temperature, pressure, space velocity) [2,13] but with implications for the yield. The future development of commercial units will be dictated by the requirements for CNFs with respect to the most successful applications.

4. Conclusions

The optimization of the operating parameters for CNF growth is an important step toward economically viable large-scale production. The present work has demonstrated that the TEOM is an excellent tool in kinetic studies of the highly dynamic process of CNF growth. Initial CNF growth rates, deactivation rates, and yield can be studied simultaneously as a function of temperature, pressure, hydrogen partial pressure, or residence time. Detailed information on deactivation processes that are normally difficult to study can be obtained as a function of TOS. Three growth periods with differing deactivation behaviors were identified when studying the decomposition of methane. The activation energy of CNF growth on relatively fresh Ni surfaces was found to be 64.6 kJ/mol, similar to what was reported for carbon diffusion on Ni (111) surfaces estimated by DFT. After an initial rapid deactivation, a stable period ascribed to steady-state growth was observed. The activation energy (92.4 kJ/mol), along with previously reported DFT calculations, suggest that the diffusion in the subsurface of a reconstructed Ni (100) and/or diffusion through supersaturated Ni bulk might be dominant at steady state. Meanwhile, a critical carbon site coverage seems to be required for the nucleation of encapsulating carbon, because of the large ensemble size required for its formation. The CNF synthesis temperature is a crucial parameter in kinetically balancing the surface reaction and dissolution/diffusion steps, to maintain a relatively low carbon site coverage on the surfaces. This was confirmed by the presence of an optimum temperature for CNF growth and an optimum hydrogen partial pressure.

The kinetic data from the TEOM experiments can be used directly for scaling up the production of CNF. For a HT-derived Ni catalyst (77 wt% Ni), there is an optimum temperature at ca. 580 °C in terms of the yield of CNF synthesis from methane. An optimum hydrogen partial pressure of ca. 0.1 bar for CNF growth in terms of initial growth rate and an optimum hydrogen partial pressure of ca. 0.4 bar in terms of yield for CNF synthesis from methane decomposition were obtained. Higher temperatures and low partial pressures of hydrogen resulted in high initial growth rates and deactivation rates. Meanwhile, low temperatures and high hydrogen partial pressures resulted in low initial growth rates and deactivation rates. A capacity of 50 g/g could be achieved at optimized conditions. Growth rates and CNF yields increased with increasing total pressure (0.3–3.8 bar). The kinetic data obtained in the TEOM reactor were verified in two micro-pilot reactors (i.e., PFR and CSTR reactors). The residence time of methane was identified as the most important parameter for process scale-up. The data on the effect of hydrogen from the TEOM were reproduced, and a successful scale-up of 10,000 times was achieved.

The present work clearly demonstrates that the TEOM reactor is a very powerful tool for the kinetic study of CNF growth that provides valuable parameters for process scale-up. The principle of the process scale-up of the CNF synthesis should also be valid for CNT CCVD synthesis from hydrocarbon decomposition. A TEOM kinetic study of ethane decomposition on Fe catalysts for CNT synthesis will be reported elsewhere.

References

[1] K.P. De Jong, J.W. Geus, Catal. Rev.-Sci. Eng. 42 (2000) 481–510.
[2] K.B.K. Teo, C. Singh, M. Chhowalla, W.I. Milne, Encyclopedia of Nanoscience and Nanotechnology, vol. 1, 2004, pp. 665–686.
[3] V.N. Parmon, G.G. Kuvshinov, V.A. Sadykov, V.A. Sobyanin, Stud. Surf. Sci. Catal. 119 (1998) 677–684.
[4] A.M. Dunker, S. Kumar, P.A. Mulawa, Int. J. Hydrogen Energy 31 (2006) 473–484.
[5] Y. Li, J. Chen, Y. Qin, L. Chang, Energy Fuels 14 (2000) 1188–1194.
[6] N.Z. Muradov, Energy Fuels 12 (1998) 41–48.
[7] P.E. Anderson, N.M. Rodriguez, Chem. Mater. 12 (2000) 823–830.
[8] L.B. Avdeeva, O.V. Goncharova, D.I. Kochubey, V.I. Zaikovskii, L.M. Plyasova, B.N. Novgorodov, S.K. Shaikhutdinov, Appl. Catal. A Gen. 141 (1996) 117–129.
[9] R.T.K. Baker, P.S. Harris, R.B. Thomas, R.J. Waite, J. Catal. 30 (1973) 86–95.
[10] D. Chen, K.O. Christensen, E. Ochoa-Fernández, Z. Yu, B. Tøtdal, N. Latorre, A. Monzon, A. Holmen, J. Catal. 229 (2005) 82–96.
[11] M.A. Ermakova, D.Y. Ermakov, Catal. Today 77 (2002) 225–235.
[12] M.A. Ermakova, D.Y. Ermakov, G.G. Kuvshinov, L.M. Plyasova, J. Catal. 187 (1999) 77–84.
[13] Z. Yu, D. Chen, B. Tøtdal, A. Holmen, J. Phys. Chem. B 109 (2005) 6096–6102.
[14] C. Pham-Huu, M.-J. Ledoux, Top. Catal. 40 (2006) 49–63.
[15] S.K. Shaikhutdinov, L.B. Avdeeva, B.N. Novgorodov, V.I. Zaikovskii, D.I. Kochubey, Catal. Lett. 47 (1997) 35–42.
[16] V.V. Chesnokov, V.I. Zaikovskii, R.A. Buyanov, V.V. Molchanov, L.M. Plyasova, Kinet. Catal. 35 (1994) 146–151.
[17] Y. Nagayasu, A. Nakayama, S. Kurasawa, S. Iwamoto, E. Yagasaki, M. Inoue, J. Jpn. Pet. Inst. 48 (2005) 301–307.
[18] P.E. Nolan, M.J. Schabel, D.C. Lynch, Carbon 33 (1995) 79–85.
[19] K. Otsuka, S. Kobayashi, S. Takenaka, Appl. Catal. A Gen. 210 (2001) 371–379.
[20] M.L. Toebes, J.H. Bitter, A.J. van Dillen, K.P. de Jong, Catal. Today 76 (2002) 33–42.

[21] W. Qian, T. Liu, Z. Wang, F. Wei, Z. Li, G. Luo, Y. Li, Appl. Catal. A Gen. 260 (2004) 223–228.
[22] C. Singh, M.S.P. Shaffer, A.H. Windle, Carbon 41 (2003) 359–368.
[23] E. Ochoa-Fernández, C. Lacalle-Vila, K.O. Christensen, J.C. Walmsley, M. Rønning, A. Holmen, D. Chen, Top. Catal. 45 (2007) 3–8.
[24] D. Chen, A. Grønvold, H.P. Rebo, K. Moljord, A. Holmen, Appl. Catal. A Gen. 137 (1996) L1–L8.
[25] D. Chen, R. Lødeng, A. Anundskas, O. Olsvik, A. Holmen, Chem. Eng. Sci. 56 (2001) 1371–1379.
[26] D. Chen, R. Lødeng, K. Omdahl, A. Anundskas, O. Olsvik, A. Holmen, Stud. Surf. Sci. Catal. 139 (2001) 93–100.
[27] V. Svrcek, I. Kleps, F. Cracioniou, J.L. Paillaud, T. Dintzer, B. Louis, D. Begin, C. Pham-Huu, M.J. Ledoux, F. Le Normand, J. Chem. Phys. 124 (2006) 184705.
[28] J.W. Snoeck, G.F. Froment, M. Fowles, J. Catal. 169 (1997) 250–262.
[29] I. Alstrup, T. Tavares, J. Catal. 139 (1993) 513–524.
[30] V.V. Chesnokov, R.A. Buyanov, Russ. Chem. Rev. 69 (2000) 623–638.
[31] G.G. Kuvshinov, Y.I. Mogilnykh, D.G. Kuvshinov, Catal. Today 42 (1998) 357–360.
[32] K. Bladh, L.K.L. Falk, F. Rohmund, Appl. Phys. A Mater. 70 (2000) 317–322.
[33] H. Neumayer, R. Haubner, Diam. Rel. Mater. 13 (2004) 1191–1197.
[34] P. Pinheiro, M.C. Schouler, P. Gadelle, M. Mermoux, E. Dooryhee, Carbon 38 (2000) 1469–1479.
[35] I. Suelves, M.J. Lazaro, R. Moliner, B.M. Corbella, J.M. Palacios, Int. J. Hydrogen Energy 30 (2005) 1555–1567.
[36] D. Venegoni, P. Serp, R. Feurer, Y. Kihn, C. Vahlas, P. Kalck, Carbon 40 (2002) 1799–1807.
[37] A. Bhattacharyya, W.-D. Chang, M.S. Kleefisch, C.A. Udovich, Application: US 97-9352095939353, 1999.
[38] DIFFRAC Plus Package, v. PROFILE PLUS, Bruker and A. GmbH, 1996.
[39] E. Ochoa-Fernández, D. Chen, Z. Yu, B. Tøtdal, M. Rønning, A. Holmen, Surf. Sci. 554 (2004) L107–L112.
[40] E.A. Blekkan, A. Holmen, S. Vada, Acta Chem. Scand. 47 (1993) 275–280.
[41] C. Park, M.A. Keane, Langmuir 17 (2001) 8386–8396.
[42] M. Del Arco, P. Malet, R. Trujillano, V. Rives, Chem. Mater. 11 (1999) 624–633.
[43] Z. Yu, Ph.D. thesis, NTNU Norway, 2005.
[44] V. Rives, S. Kannan, J. Mater. Chem. 10 (2000) 489–495.
[45] B. Scheffer, P. Molhoek, J.A. Moulijn, Appl. Catal. 46 (1989) 11–30.
[46] G. Fornasari, M. Gazzano, D. Matteuzzi, F. Trifiro, A. Vaccari, Appl. Clay Sci. 10 (1995) 69–82.
[47] T.V. Reshetenko, L.B. Avdeeva, Z.R. Ismagilov, A.L. Chuvilin, V.A. Ushakov, Appl. Catal. A Gen. 247 (2003) 51–63.
[48] J.W. Snoeck, G.F. Froment, M. Fowles, J. Catal. 169 (1997) 240–249.
[49] D. Chen, E. Bjørgum, K.O. Christensen, A. Holmen, Adv. Catal. 51 (2007) 351–382.
[50] J.B. Nagy, G. Bister, A. Fonseca, D. Mehn, Z. Konya, I. Kiricsi, Z.E. Horvath, L.P. Biro, J. Nanosci. Nanotechnol. 4 (2004) 326–345.
[51] F. Abild-Pedersen, J.K. Nørskov, J.R. Rostrup-Nielsen, J. Sehested, S. Helveg, Phys. Rev. B 73 (2006) 115419.
[52] H.S. Bengaard, J.K. Nørskov, J. Sehested, B.S. Clausen, L.P. Nielsen, A.M. Molenbroek, J.R. Rostrup-Nielsen, J. Catal. 209 (2002) 365–384.
[53] J. Rostrup-Nielsen, D.L. Trimm, J. Catal. 48 (1977) 155–165.
[54] R.T. Yang, J.P. Chen, J. Catal. 115 (1989) 52–64.
[55] S. Helveg, C. Lopez-Cartes, J. Sehested, L.P. Hansen, B.S. Clausen, R.J. Rostrup-Nielsen, F. Abild-Pedersen, J.K. Nørskov, Nature 427 (2004) 426–429.
[56] V.I. Zaikovskii, V.V. Chesnokov, R.A. Buyanov, Appl. Catal. 38 (1988) 41–52.
[57] Y.-A. Zhu, X.-G. Zhou, D. Chen, W.-K. Yuan, J. Phys. Chem. C 111 (2007) 3447–3453.
[58] Y.-A. Zhu, Y.-C. Dai, D. Chen, W.-K. Yuan, Carbon 45 (2007) 21–27.
[59] M.C. Demicheli, E.N. Ponzi, O.A. Ferretti, A.A. Yeramian, Chem. Eng. J. 46 (1991) 129–136.
[60] M.A. Ermakova, D.Y. Ermakov, L.M. Plyasova, G.G. Kuvshinov, Catal. Lett. 62 (1999) 93–97.
[61] E.S. Steigerwalt, G.A. Deluga, C.M. Lukehart, J. Phys. Chem. B 106 (2002) 760–766.
[62] C.A. Bessel, K. Laubernds, N.M. Rodriguez, R.T.K. Baker, J. Phys. Chem. B 105 (2001) 1115–1118.
[63] V.V. Chesnokov, I.P. Prosvirin, N.A. Zaitseva, V.I. Zaikovskii, V.V. Molchanov, Kinet. Catal. 43 (2002) 838–846.
[64] M. Menon, A.N. Andriotis, G.E. Froudakis, Chem. Phys. Lett. 320 (2000) 425–434.
[65] I. Kvande, S.T. Briskeby, M. Tsypkin, M. Rønning, S. Sunde, R. Tunold, D. Chen, Top. Catal. 45 (2007) 81–85.